Synthesis, experimental and molecular dynamics simulation of the ESI-CID spectrum of the nerve agent Novichok analog O-2-methoxyethyl N-[bis(dimethylamino)methylidene]-P-methylphosphonamidate

Taynara Carvalho-Silva,[a,*], Lucas Modesto-Costa,[a] Caio V. N. Borges,[a,b], Samir F. A. Cavalcante,[b,c] Roberto B. Sousa,[d] Antonio L. S. Lima,[a], Itamar Borges Jr[a,*]

[a] *Departamento de Química, Instituto Militar de Engenharia (IME), Praça General Tibúrcio 80, 22290-270 Rio de Janeiro-RJ, Brazil*

[b] *Instituto de Defesa Química, Biológica, Radiológica e Nuclear (IDQBRN), Exército Brasileiro, Avenida das Américas 28705, Área 4, 23020-470 Rio de Janeiro-RJ, Brazil*

[c] *Department of Chemistry, Faculty of Science, University of Hradec Králové (UHK), Rokitanského 62/26, 500 03 Hradec Králové, Czech Republic*

[d] *Ministério da Ciência, Tecnologia e Inovação, Coordenação-Geral de Bens Sensíveis (CGBS), SPO - Área 5 - Quadra 3 - Bloco E, 20610-200 Brasília – DF, Brazil*

KEYWORDS: Novichok, A-242, fragmentation pathways, mass spectrometry, molecular dynamics

*E-mail: itamar@ime.eb.br

ABSTRACT: The comprehensive and accurate analysis of mass spectral data is critical for the unequivocal identification of environmental samples containing compounds short-listed by the Chemical Weapons Convention (CWC). In particular, experiments with nerve agents are limited by the high risks involved in their handling. Therefore, the possibility of studying fragmentation pathways by a theoretical approach is especially welcome. In this work, for the first time, O-2-methoxyethyl N-[bis(dimethylamino)methylidene]-P-methylphosphonamidate, an analog of the Novichok nerve agent A-242, was synthesized employing a one-pot microscale synthesis. Electron ionization (EI) and electrospray ionization (ESI) mass spectrometry (MS) spectra were measured to produce data for CWC verification purposes. Considering that ESI-MS/MS is a powerful method for analyzing non-volatile, highly polar, and very water-soluble compounds, such as degradation products of nerve agents, we extensively investigated for the first time the ESI-(collision-induced dissociation) CID fragmentation pathways of the selected molecule. For this purpose, molecular dynamics simulations using the Quantum Chemical Mass Spectrometry (QCxMS) method employing the semiempirical electronic structure method GFN2-xTB were compared with Triple Quadrupole electrospray ionization (ESI) experimental spectra in positive ion mode. The base peak of the EI spectrum for this molecule was found to be m/z 151, which strongly suggests a McLafferty +1 rearrangement involving the 2-methoxyethyl moiety. According to the simulations, the formation of the m/z 106 ion in the ESI-CID spectrum results from the rearrangement involving a transfer of one dimethylamino group to the phosphorus atom. This mechanism would be difficult to identify without employing theoretical methods.

1 INTRODUCTION

Chemical Warfare Agents (CWAs) are any toxic chemical or its precursors that can cause death, injury, temporary incapacitation, or sensory irritation through its chemical action in humans or animals [1]. These substances, some of which have been used in different conflicts and assassination attempts [2], are under strict regulation by the Convention on the Prohibition of the Development, Production, Stockpiling, and Use of Chemical Weapons and their Destruction (Chemical Weapons Convention, CWC), listed on its Annex on Chemicals [1].

The toxic chemicals in the CWC are potent acetylcholinesterase inhibitors, some classified as organophosphorus nerve agents (OPNAs), whose acute exposure can cause rapid death [3]. Until recently, these agents were commonly separated in the literature into two main groups: G-series and V-series [4]. However, the disclosure of once elusive compounds secretly developed in the Soviet Union during the Cold War [5] codenamed Novichok agents gave rise to the so-called A-series [6].

The first information concerning Novichok was revealed in the early 90's [7]. The recent assassination attempts of a former Russian spy and his daughter in 2018 and an opponent of the Russian government in 2020 [8,9] boosted the efforts to add these chemicals to CWC [10,11]. An amendment, the first since the CWC was upheld in 1997, took effect on June 2020 and included new organophosphorus and carbamates that can act as nerve agents [12]. However, it should be clear that even prior to the addition of these nerve agents, their use as chemical weapons was already prohibited by the CWC [10]. Therefore, the main purpose of an addition to the Annex on Chemicals is to assist the CWC implementation and its verification regime.

The precise identification of chemicals of concern in a variety of environmental samples [13] is required to comply with the verification regime; the techniques of gas or liquid

chromatography (GC or LC) coupled with mass spectrometry (MS) or tandem mass spectrometry (MS/MS) are the primary tools for this task [14]. GC-MS analysis is typically performed under electron ionization (EI) conditions, which is the oldest and still the most used ionization technique for the analysis of CWC-related chemicals [15]. Other ionization techniques, such as chemical ionization (CI), are also used [16].

More recently, several studies focused on the analysis of degradation products of CWA by LC-MS [17–19], which is preferably performed in the electrospray ionization (ESI) mode for this type of chemicals [16]. In this ionization process, the ions of the investigated molecule are generated either by protonation or adduct formation in the positive ion mode, or deprotonation in the negative ion mode, which produces closed-shell (even-electron) ions [20,21]. As ESI does not typically results in much in-source fragmentation, hence is a soft ionization method [20], it is usually combined with collision-induced dissociation (CID), in which fragmentation is induced by collision with molecules of an inert gas [22]. The collision excites the initial ions (precursor ions) which break up into fragment ions (product ions), generating a MS^2 (or MS/MS) spectrum [23].

The LC-MS and LC-MS/MS techniques have opened up the possibility of performing direct analysis of aqueous samples and a greater suitability over GC-MS for the analysis of non-volatile, highly polar, and very water-soluble compounds, such as degradation products of nerve agents [14,24]. In addition to the advantages above, the need for at least two different spectrometric techniques [16,25] for producing a reliable result makes them crucial for laboratories involved in analyzing CWAs samples to address and successfully complete their analytical task [14].

Unfortunately, as LC-MS and LC-MS/MS are very instrumentation dependent [14] and establishing in-house spectral libraries for CWC-related chemicals implies dealing with

molecules of limited access and high toxicity [26,27]. For these reasons, a safe and rational alternative to determine their mass spectra is to employ computational quantum chemical simulation methods [28], such as the Quantum Chemical Mass Spectrometry method (QCxMS) developed by Grimme's group [29]. The program is based on molecular dynamics (MD) simulations, first introduced by Hase and coworkers in the context of mass spectrometry [30–32], and addresses the problem of lack of information on the fragmentation dynamics that compromises static theoretical methods while avoiding the necessity of large databases necessary for machine learning algorithms [33].

Several works have demonstrated the accuracy of the QCEIMS method in simulating mass spectra of different types of molecules [29,31,34,35], and in particular, the first application to CWAs by our group [26,36]. Recently, the QCEIMS program extended to determine CID spectra was renamed as QCxMS [37–39]. Although MD methods to simulate CID experiments have been proposed before [33,40–43], now explicit collisions between ions and collision gas could be included in a friendly and accurate software specifically designed to determine CID mass spectra from MD simulations [37].

Notably, for Novichoks, a theoretical approach is supported by different works [18,36,38,44–49]. However, we did not find computational studies involving the simulation of the CID mass spectra of nerve agents or their analogs. Therefore, in this work we investigate the mass spectra of the O-2-Methoxyethyl N-[bis(dimethylamino)methylidene]-P-methylphosphonamidate molecule (Figure 1) using the QCxMS method in positive ion CID mode, and the results were compared with ESI-CID measurements. We synthesized the Novichok analog through a one-pot microscale synthetic procedure to determine novel EI-MS and ESI-MS/MS data. This molecule is encompassed by Schedule 2.B.04 of the CWC and is an expected degradation product of the A-242 resulting from the use of DS-2 decontaminant,

except that it features 1,1,3,3-tetramethylguanidine substituents instead of the 1,1,3,3-tetraethylguanidine of the actual agent. The most significant fragmentation pathways will be discussed and used to rationalize the mass spectrum.

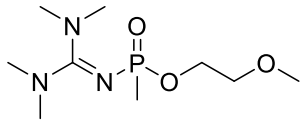

Figure 1 - O-2-methoxyethyl N-[bis(dimethylamino)methylidene]-P-methylphosphonamidate

2 MATERIALS AND METHODS

2.1 Reagents and chemicals

All chemicals in this work were purchased from commercial suppliers and used as received. 1,1,3,3-tetramethylguanidine, 2-methoxyethanol, dry triethylamine, N,N-Diisopropylethylamine (DIPEA, Hünig's base) and inorganic compounds (60% sodium hydride in mineral oil, phosphate salts for buffer solutions, anhydrous sodium sulfate, molecular sieves) were purchased from Sigma Aldrich Brasil (São Paulo, Brazil). Dichloromethane was purchased from Anidrol (Diadema, São Paulo State, Brazil) and dried over 4Å molecular sieves activated at 150 °C for 8 hours. Methylphosphonic dichloride was synthesized at IDQBRN (Instituto de Defesa Química, Biológica, Radiológica e Nuclear), and the analytical data were consistent with the literature. Acetonitrile and water for the LC-MS/MS runs were purchased from Merck Brasil (São Paulo, Brazil). Deuterated chloroform (1% tetramethylsilane as internal standard) was purchased from Cambridge Isotopes Laboratories (Tewksbury, Massachusetts, USA).

2.1 Microscale synthesis procedure

To a 7mL dry vial (dry oven, 30min at 130°C) equipped with a magnetic stirrer, methylphosphonic dichloride (50 mg, 1.0 eq.) and 1 mL of dichloromethane were added, cooled to 0 °C with the aid of an ice bath. To this mixture, were slowly added DIPEA (130,6 µL, 2.0 eq.) and 1,1,3,3-tetramethylguanidine (TMG, 47,7 µL; 1.0 eq.) in 1 mL of dichloromethane. White vapors evolved during the addition of amines, probably due to the formation of quaternary ammoniums.

After 2 hours (with the reaction followed by GC-MS for verifying consumption of methylphosphonic dichloride), a suspension of dichloromethane (1 mL), the corresponding alcohol (1.0 eq.) and sodium hydride (30.1 mg, 60% in mineral oil, 2.0 eq., pretreated with hexane to remove mineral oil) was added cautiously at 0 °C. After four hours of reaction (monitored by GC-MS and LC-MS), the reaction was left at room temperature, and after sedimentation of solids, the reaction mixture was filtered through a syringe filter (0.22 microns), transferred to a tared 7 mL vial, and slowly evaporated in a rotary evaporator (bath at 40 °C), yielding a yellow oil. As they are potential cholinesterase inhibitors, the products have not been purified to avoid toxicity risks for all operators. The summary description of the synthesis method is illustrated in Figure 2.

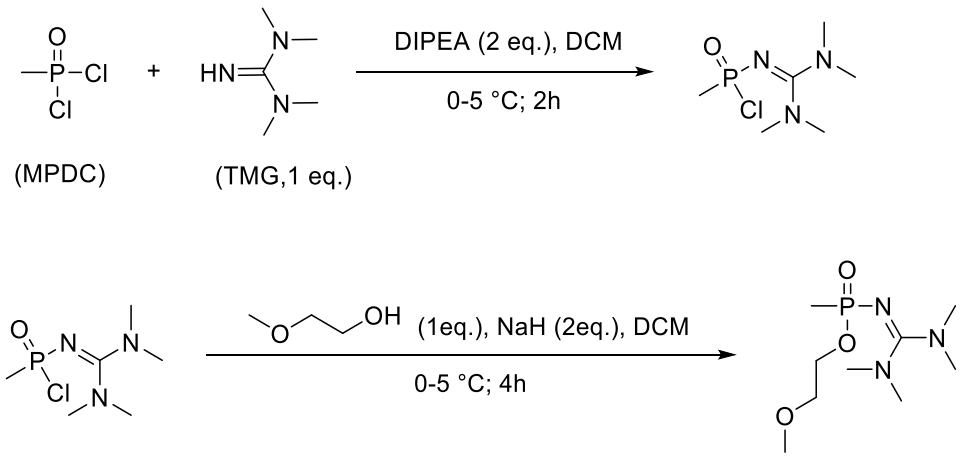

Figure 2 - General method for the micro synthesis of O-2-methoxyethyl N-[bis(dimethylamino) methylidene]-P-methylphosphonamidate

2.3 GC/MS analysis

GC-MS analyses were performed using an Agilent 6890N gas chromatograph equipped with a 5973 quadrupole mass selective detector (MSD; Agilent Technologies, Inc., Santa Clara, CA, USA), a HP-5MS (5% phenyl, 95% dimethylpolysiloxane, Agilent's J&W Scientific) capillary column (30 m, 320 mm i.d. and 0.25 mm film thickness), and helium as the carrier gas at constant flow rate of 1.8 mL min-1. The oven temperature was set at 40 °C for 3 min, then ramped to 280 °C at 10 °C/min and held for 6 min. The samples were injected in splitless mode at an injection temperature of 250 °C. The temperatures of the EI source and analyzer were kept at 230 and 150 °C, respectively. The scan range was *m/z* 35–500.

2.4 LC-MS/MS analyses

An Agilent 1260 Infinity HPLC System equipped with a 50 mm x 2.1 mm x 1.8µm ACE Generix C18 column was used for the LC analysis. The mobile phase consisted of water (solvent A) and acetonitrile (solvent B), each modified with 0.1% formic acid. The gradient was as follows: 5% B at 0 min, linear increase up to 90% B at 5 min, linear decrease to 5% of B at 10 min, and hold for 5 min. The flow rate was set at 0.2 mL/min. The injection volume for all LC experiments was set to 10 µL and achieved using an autosampler.

The LC column effluent was introduced on an Agilent 6410B triple quadrupole mass spectrometer. The source settings were as follows: spray voltage, +4000 V; capillary temperature, 300°C; drying gas (nitrogen) 6L/min; nebulizer gas pressure 15 psi; fragmentor voltage of 70V; Cell Acceleration Voltage 5V and collision energy of 8 eV. MassHunter

software v.8.0 (Agilent, San Jose, CA, USA) was used for instrument control, data acquisition, and data handling.

2.5 NMR analysis

NMR spectral acquisition employed a Bruker Advance III Plus NMR spectrometer equipped with a 400 MHz magnet UltraShield™ 400 Plus. All NMR spectra acquisition and pre-processing were performed under the control of a workstation with TopSpin 2.4 software. A sample consisting of the crude product in deuterated chloroform ($CDCl_3$) was used for ^{1}D ^{1}H-^{31}P HSQC experiment. The obtained data spectra were referred to as tetramethylsilane.

2.6 Molecular dynamics simulation

Before running the QCxMS simulations, as advised by the program's developers, the protonation of the targeted species was determined using the automated protonation protocol [29] of the Conformer Rotamer Ensemble Sampling Tool (CREST) [50–52] version 2.11, which employs the semiempirical electronic structure GFN2-xTB method [53]. Afterward, the most populated protonated structures inside a 30 kcal/mol energy range were re-optimized at the density functional theory (DFT) level using the exchange-correlation functional PBEh-3c [54] with the def2-mSVP[55] basis function set, employing the CENSO [56] script version 1.2.0. The DFT calculations employed the ORCA [57–59] suite of programs version 4.2.1 to yield more accurate gas phase energies while maintaining a low computational cost [51].

The CID calculations were computed by QCxMS [37] version 5.0.3 using the xTB [60] version 5.8.1 on AMD Ryzen 7 3800X 3.9GHz computer cores of in-house cluster. The standard parameters of the program, except that molecular nitrogen was used as the collision gas instead of argon, were employed.

In the QCxMS simulations, the protonated input structure is first equilibrated at a constant default temperature of 500 K. An ensemble of snapshot geometries is collected along a sampling MD preliminary step to be used as initial geometries for the following fragmentation simulations known as production runs. In this work, the simulation of the CID process in the production runs was done with the recommended general activation run [37], with fragmentation being induced by thermal heating, collisional activation, and consecutive mean-free-path MD simulations. This extensive step is parallelized, and each production run is executed on a single computer core, as briefly described in the following paragraphs.

The thermal heating step scales the internal energy of the protonated system to a value inside a range that depends on the molecule size to mimic the ESI process. This value is randomly varied for each production run to account for variations in the experiment. Afterward, consecutively, multiple collision simulations are performed, with the number of collisions calculated according to kinetic gas theory applied to the collision chamber properties, and whose default values are the collision gas pressure of 0.132 Pa, collision gas temperature of 300K, and collision cell length of 0.125 m.

For the collision simulation, the gas molecule is placed along a Cartesian axis 25 Å away from the protonated molecule center of mass and considered stationary. Its position is displaced perpendicular to this vector by a random value to account for a varying scattering angle, better known as the impact parameter b, which has the maximum radius value of $[M+H]^+$ to avoid insignificant collisions. The velocity of the precursor ion after the acceleration in the electric field of the collision cell is calculated from the chosen collision energy (E_{LAB}).

After a collision event finishes, the simulation runs for 800 more MD time steps to guarantee that the interactions between the collision partners decayed. The ion is propagated in time to enable the energy redistribution of the impact energy into its rovibrational modes. The

default value between multiple collisions is set to 5 ps. If the ion undergoes fragmentation, the vertical ionization potentials of the fragments are calculated by the ΔSCF (self-consistent field) method [61], and the fragment with the highest statistical charge is further propagated in a subsequent MD simulation to account for complete energy distribution. The external Plot Mass Spectrum (PlotMS) program [62] is used for counting the fragments and plotting the theoretical spectrum.

The MD calculations in QCxMS employ the semiempirical GFN2-xTB electronic structure method in combination with the finite electronic temperature (Fermi smearing) model [39,63]. The electronic temperature for the ground state sampling is set to 298 K and increased to 5000 K for the production runs. MD steps employed the leap-frog algorithm with a time step of 0.5 fs. A good statistical convergence of the spectral results is obtained with a number of trajectories equal to 25 times the number of atoms per molecule [37], which resulted in 975 trajectories for our molecule. The equilibration MD and the snapshot sampling were set to 50 fs times the number of trajectories. The default energy in the laboratory reference frame (E_{LAB}) is set to 40 eV, higher than the experimental, as advised by the developers [64].

3 RESULTS AND DISCUSSION

3.1 Synthesis and MS data of O-2-methoxyethyl N-[bis(dimethylamino)methylene]-P-methylphosphonamidate

An LC-MS analysis of the crude reaction mixture indicated the formation of at least three possible by-products (Figure 3): N-(bis(dimethylamino)methylene)-P-methylphosphonamidic acid (BP1), bis(2-methoxyethyl) methylphosphonate (BP2) and 2-(((bis(dimethylamino)methylene)amino) (methyl)phosphoryl)-1,1,3,3-tetramethylguanidine (BP3). The formation of these by-products was further confirmed by a tandem MS/MS analysis,

presenting fragmentation profiles that are consistent with these structures. Moreover, there were present the impurities of 1,1,3,3-tetramethylguanidine (TMG) and N,N-Diisopropylethylamine (Hunig's base).

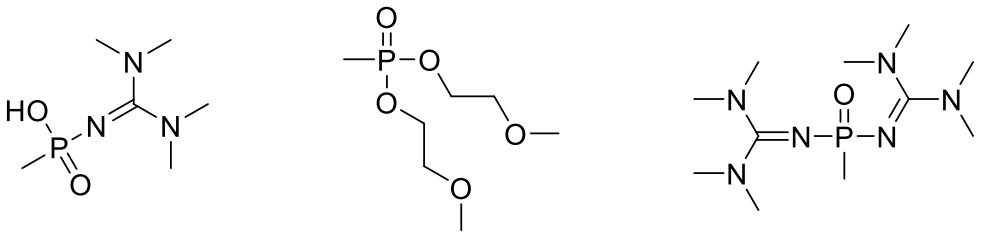

BP1 [M+H]$^+$ *m/z* = 194 | BP2 [M+H]$^+$ *m/z* = 213 | BP3 [M+H]$^+$ *m/z* = 291

Figure 3 - Major by-products that were formed in the crude reaction mixture.

The separation and purification of CWC-related compounds are very difficult due to their extreme toxicity, so we decided not to purify the O-2-methoxyethyl N-[bis(dimethylamino)methylene]-P-methylphosphonamidate. Since recording NMR data requires a pure compound, we could only infer the presence of our compound of interest and the significant impurities containing a P-CH_3 in their structure through the selectivity of a 1D ^{1}H-^{31}P HSQC experiment. In this type of analysis, signals from protons with a scalar coupling to a ^{31}P nuclei are observed exclusively. In contrast, the signals from the sample background of obscuring signals from organophosphorus compounds in ^{1}H NMR spectra are efficiently removed.

Attention was then focused on the EI spectrum of O-2-methoxyethyl N-[bis(dime thylamino)methylene]-P-methylphosphonamidate (Figure 4). Major EI fragment ions for this molecule are also illustrated in Figure 5 and were primarily based on the fragmentation scheme proposed in the literature [13].

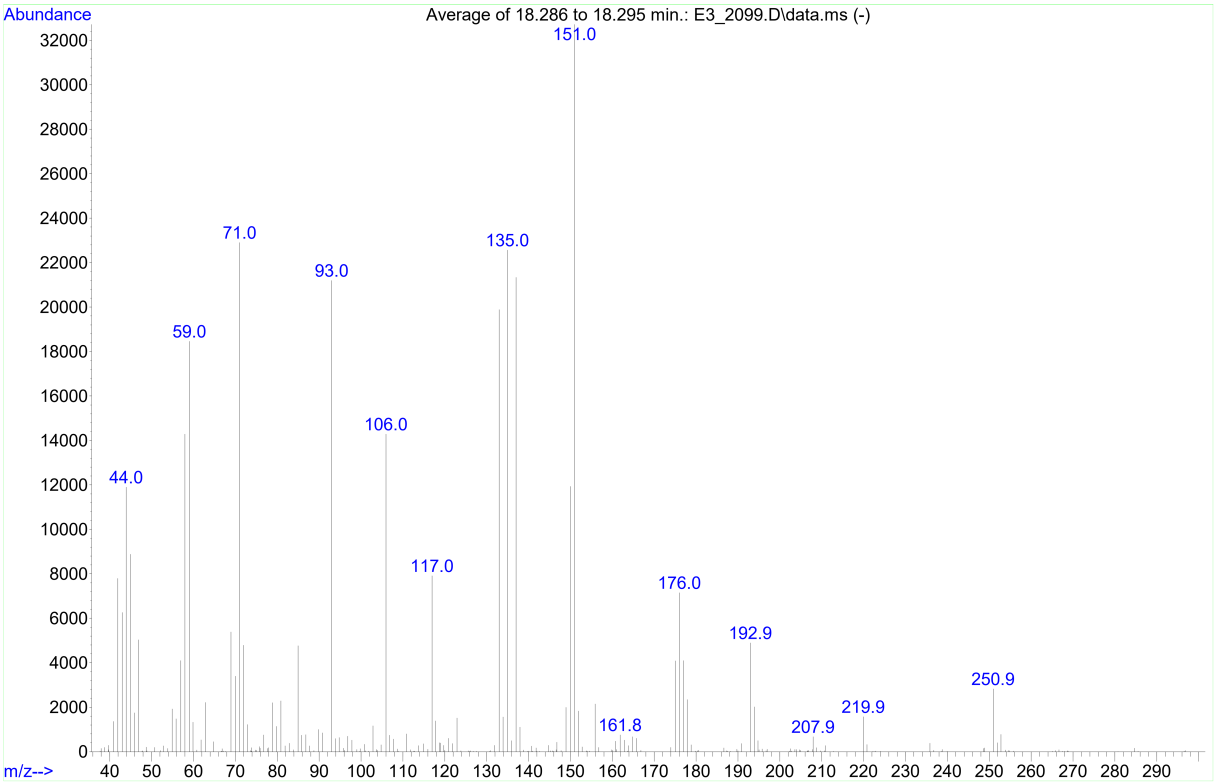

Figure 4 - EI mass spectra of O-2-Methoxyethyl N-[bis(dimethylamino)methylidene]-P-methyl phosphonamidite.

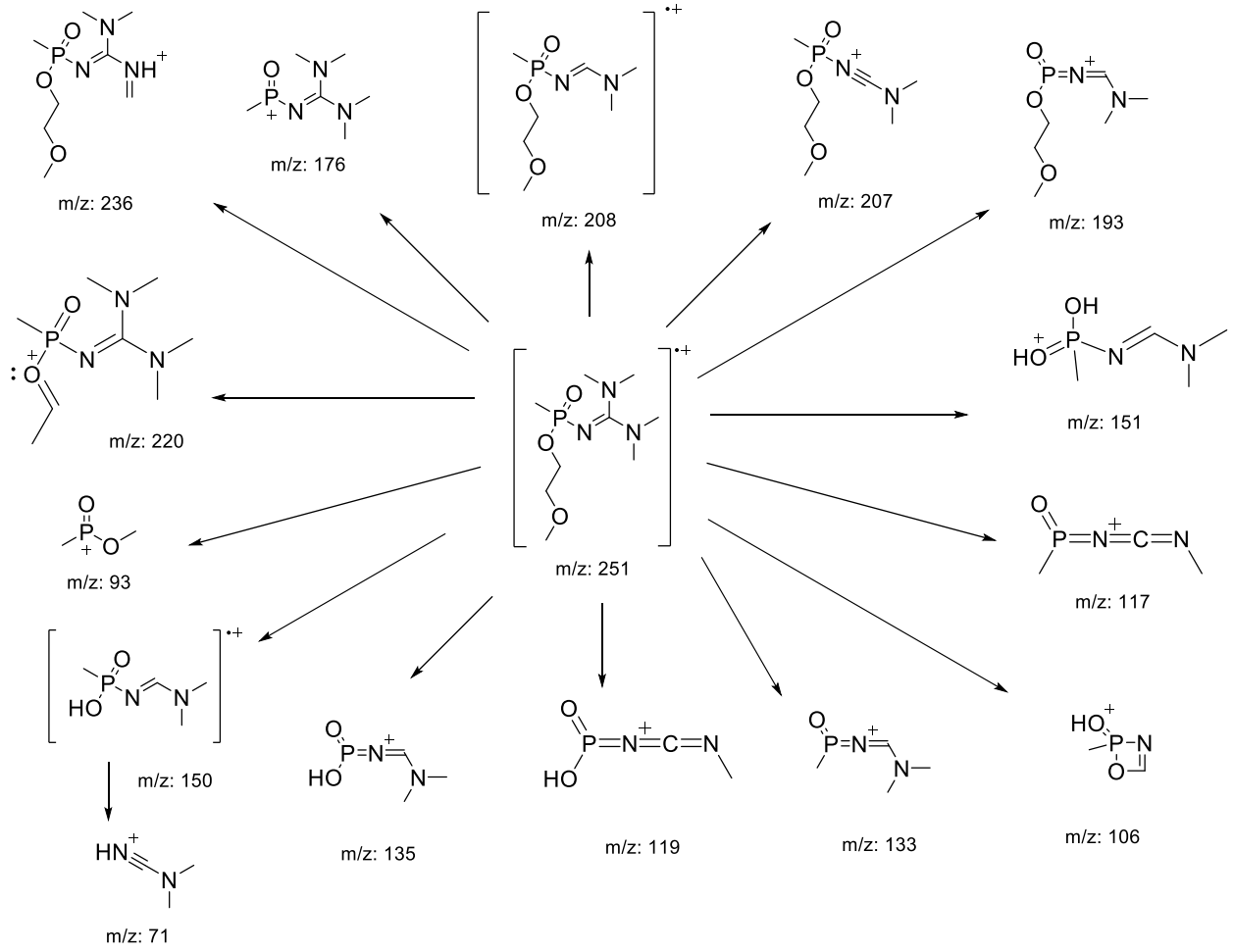

Figure 5 - General EI-MS fragmentation pattern of O-2-methoxyethyl N[bis(dimethylamino) methylidene]-P-methylphosphonamidate.

The main difference found in relation to the spectra already reported [13] for this class of compounds is the base peak of the spectrum at *m/z* 151, which strongly suggests the occurrence of a McLafferty +1 (ML+1) rearrangement from the *m/z* 208 radical cation, involving the longer carbon chain bonded to the oxygen atom (Figure 6).

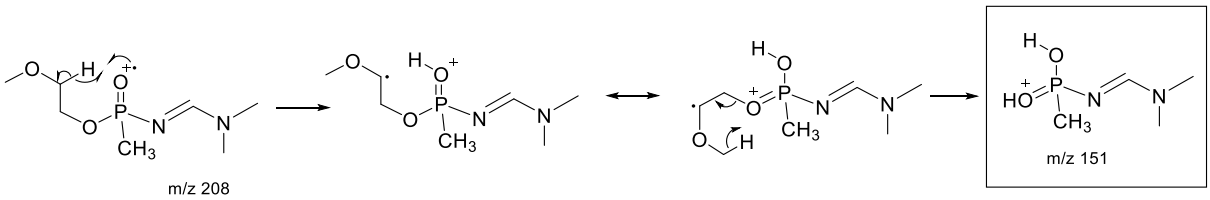

Figure 6 - Proposed McLafferty +1 rearrangement generating ion *m/z* 151.

Both *m/z* 150 and *m/z* 151 can then produce the fragment of *m/z* 117 (Figure 7), which despite having appeared in the spectra already reported in the literature [13], this time has a slightly more pronounced intensity. Furthermore, given the possibility of forming the radical cation on the oxygen from the 2-methoxyethyl chain, the ion of *m/z* 220 can be created by the expulsion of a methoxy radical (Figure 8).

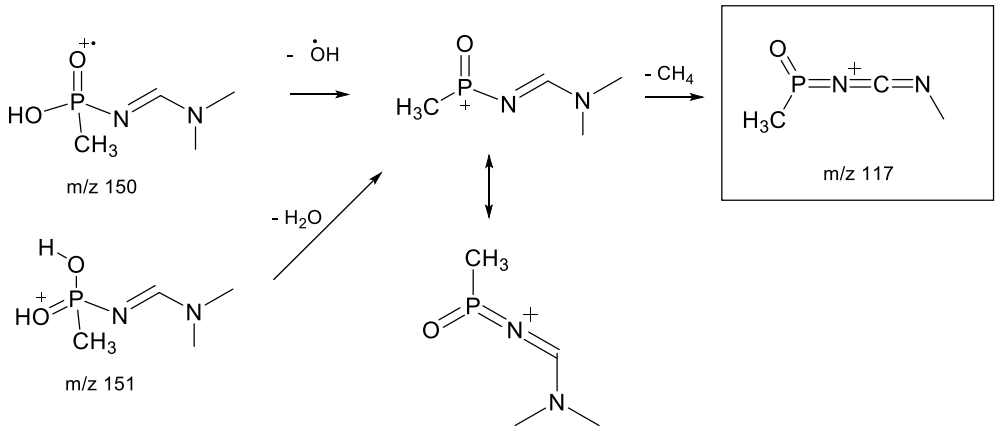

Figure 7 - Proposed formation mechanisms for ion *m/z* 117 from *m/z* 150 and *m/z* 151 fragments.

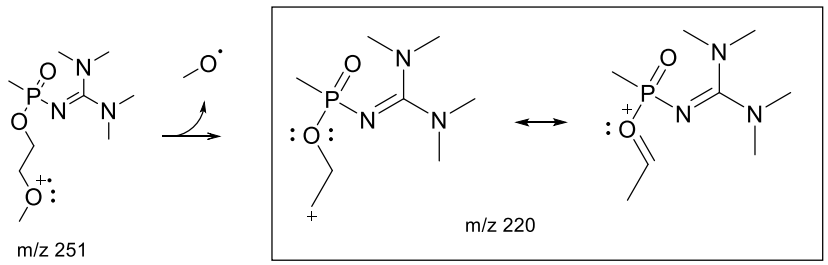

Figure 8 - Proposed mechanism of formation for ion *m/z* 220.

With the promising results from the EI spectrum, we moved on to an extensive study of the ESI-CID results. The experimental ESI spectrum of O-2-methoxyethyl N-[bis(dimethylamino)methylene]-P-methylphosphonamidate is shown in Figure 9. The discussion of fragmentation pathways will be carried out in the next section employing the data generated by the simulations.

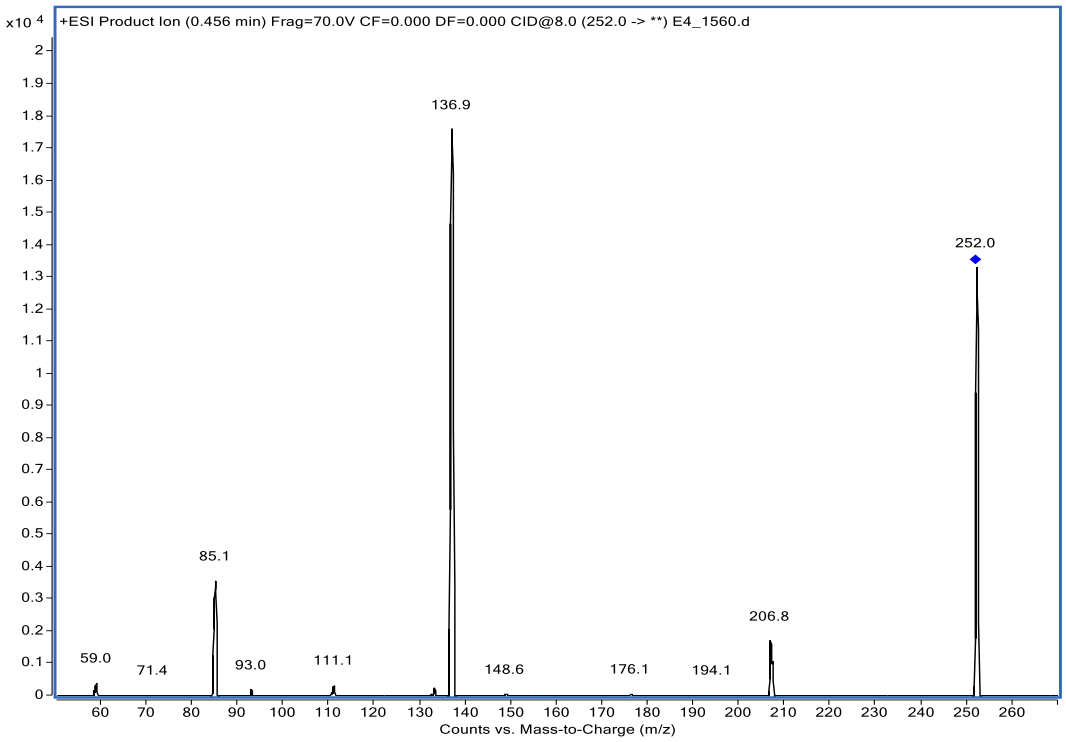

Figure 9 - Positive ESI Product ion mass spectra of O-2-methoxyethyl N-[bis(dimethylamino)methylidene]-P-methylphosphonamidate.

3.2 Comparison between calculated and experimental spectra

Fragmentation pathways in ESI-CID are usually classified according to the retention of the charge [22,23]. Charge retention fragmentations (CRF) produce fragment ions with the charge located at the same site of its precursor ion when the bond cleavage location is physically remote from the location of the charge and without direct participation in the mechanism. In contrast, charge migration fragmentations (CMF) occur by displacement of the charge, usually eliminating the initial charge site moiety as a neutral molecule [22,23]. Since the precursor ion in the ESI positive ion mode is the protonated molecule, the initial location of the additional proton (charge) significantly influences the resulting spectrum [37].

For the O-2-methoxyethyl N-[bis(dimethylamino)methylidene]-P-methylphos phonamidate molecule (M = 251.2 Da, $C_9H_{22}N_3O_3P$), CREST computed three distinct protomer structures populated in the 30 kcal/mol free energy range at 600 K, which contributed most to the final spectrum. However, as more protonated structures are possible in a classical protonation formalism, we also investigated one additional protomer spectra, which provided additional information on the fragmentation mechanisms. We note that more than one conformer was generated for some protonated species. Since the protonation sites are necessary for the QCxMS calculations, we only considered the most stable found conformer for each protomer (Figure 10).

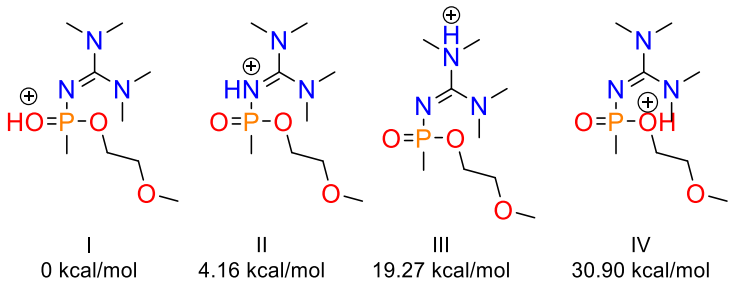

Figure 10 - Protomers I-V of the O-2-methoxyethyl N-[bis(dimethylamino) methylidene]-P-methylphosphonamidate molecule with their assigned relative energies Gtot [kcal/mol] to the most stable structure protomer I (0.0 kcal/mol) obtained by PBEh-3c DFT calculations.

The combined spectrum of the protomers calculated with QCxMS is compared to the experimentally measured spectrum in Figure 11. However, since the collision process considerably increases the internal energy of these ions, thus allowing proton mobility, the exact population and the influence of the protomers on the final spectrum cannot be based solely on free energies values [38].

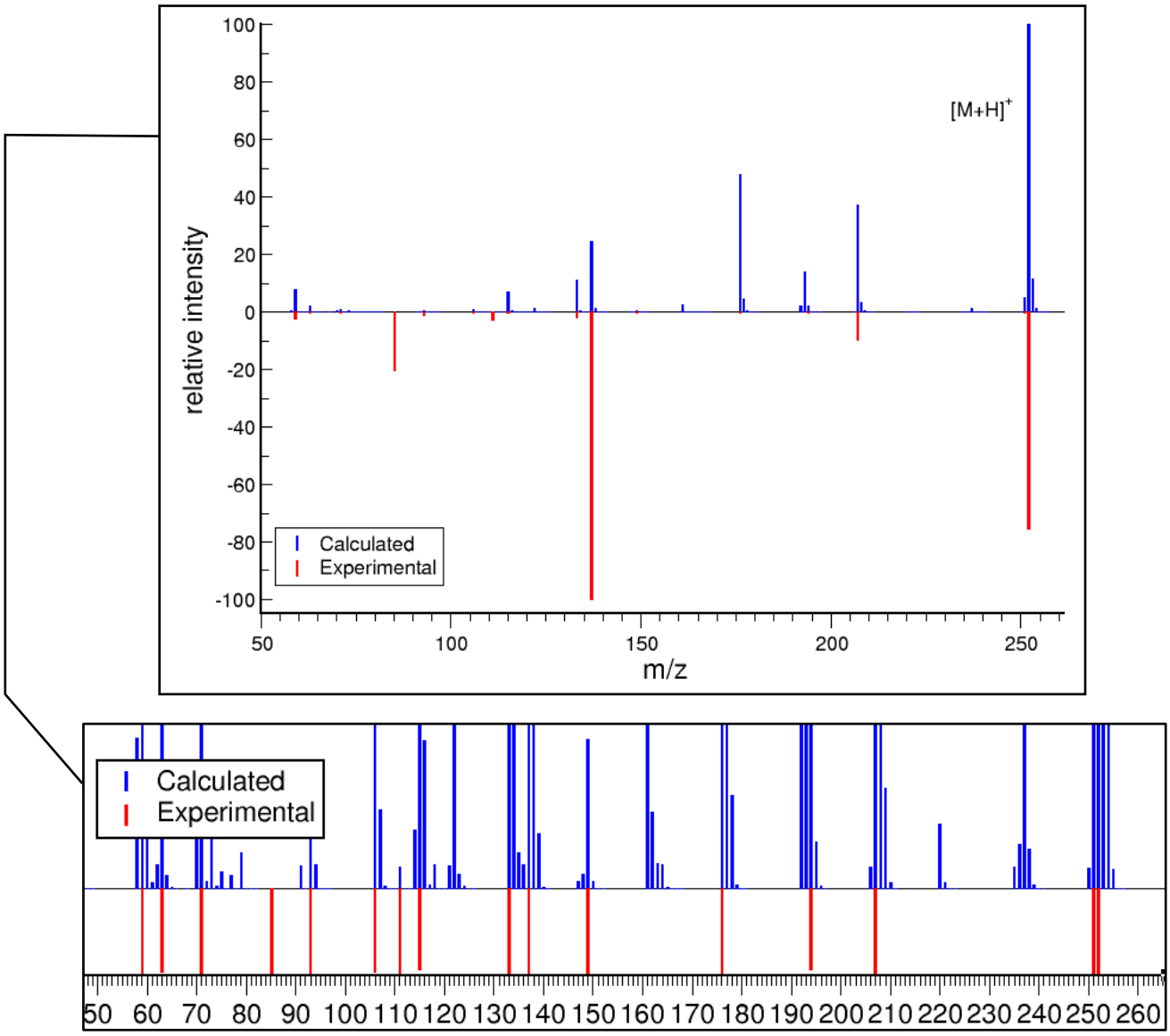

Figure 11 - Combined spectrum of the protomers calculated with QCxMS (blue) compared to the experimentally measured spectrum (red).

The experimental MS/MS spectrum of the investigated compound presents a very intense *m/z* 137 ion and several characteristic ions with very low intensities, which were all included to improve the comprehensiveness of our ESI/MS study. The QC calculations identified 14 out of the 15 fragments generated by the mass spectrometer, resulting in a coverage of 93.3% of the signals (Table 1, column simulated). More importantly, our theoretical

approach provided in detailed these pathways, which would typically require a considerable amount of time and experience, especially if multiple protomer structures are considered [38]. To illustrate the mechanistic details of the proposed fragmentation pathways for the O-2-methoxyethyl N-[bis(dimethylamino)methylidene]-P-methylphosphonamidate, standard fragmentation rules were used (Figure 12).

Table 1 - Fragment list. Fragments measured by ESI-MS/MS are listed according to their molecular mass. Fragments simulated by QCxMS are marked.

Fragment No.	Measured fragments (*m/z*)	Simulated
1	59	yes
2	63	yes
3	71	yes
4	85	no
5	93	yes
6	106	yes
7	111	yes
8	115	yes
9	133	yes
10	137	yes
11	149	yes
12	176	yes
13	194	yes
14	207	yes
15	251	yes

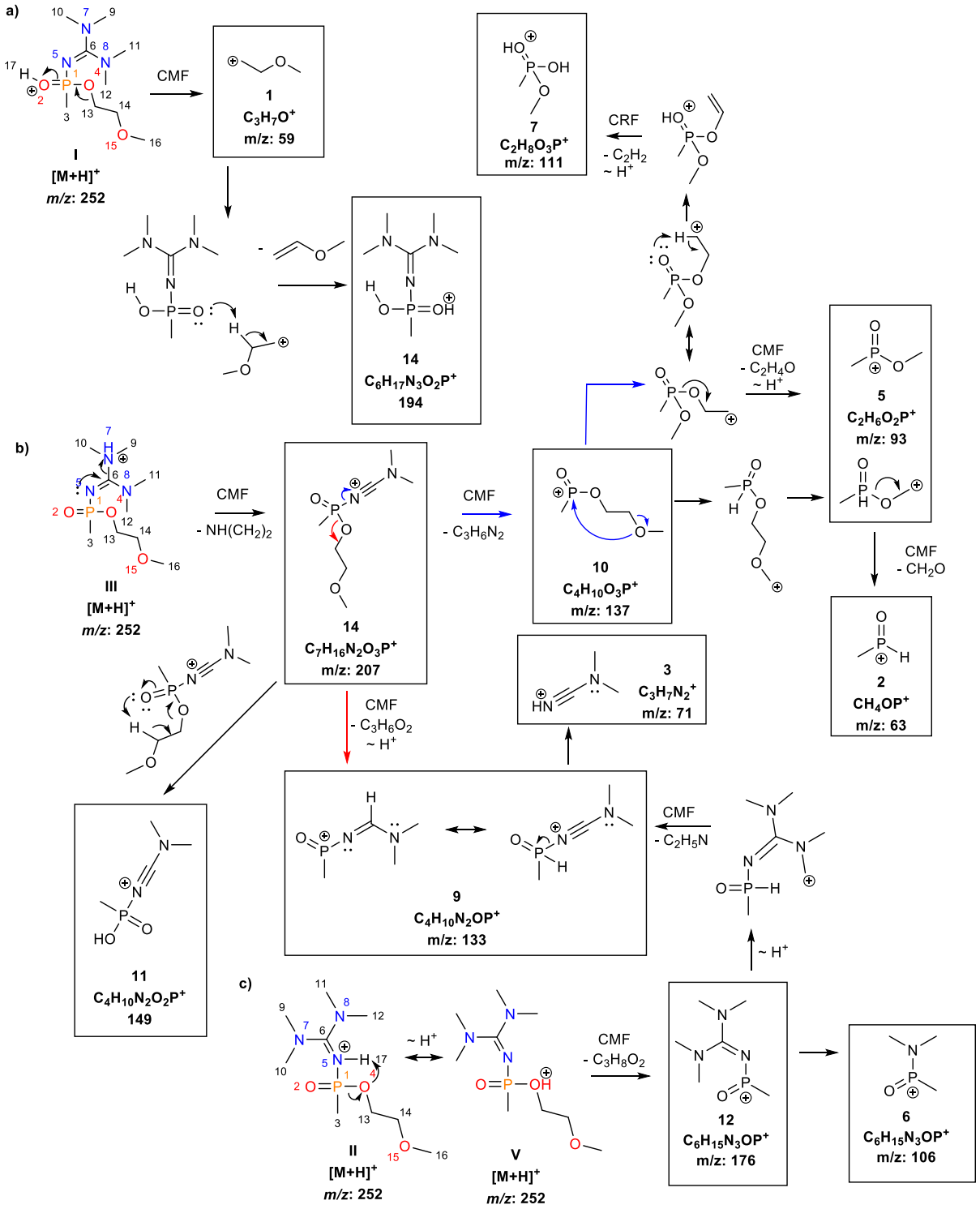

Figure 12 - Proposed fragmentation pathways of O-2-methoxyethyl N-[bis(dimethylamino)methylidene]-P-methylphosphonamidate. ~ H+ means proton migration. Boxed fragments were experimentally detected. Unboxed structures are "snapshots" of the calculated trajectories and are displayed for clearer retracing the reaction pathways; they are

not global minima on the potential energy surface. For clarity, the neutral fragment has not been depicted in all cases.

From Protomer I, the $C_3H_7O^+$ (*m/z* 59) fragment is generated in a CMF reaction by the cleavage of the O4-C13 bond. If geometric and energetic conditions are favorable, the $C_6H_{17}N_3O_2P^+$ (*m/z* 194) ion can be generated by a proton transfer from the *m/z* 59 ion to the oxygen bonded to phosphorus of the *m/z* 193 neutral molecule fragment in a mechanism similar to the one proposed for organophosphorus esters (Figure 13) [65].

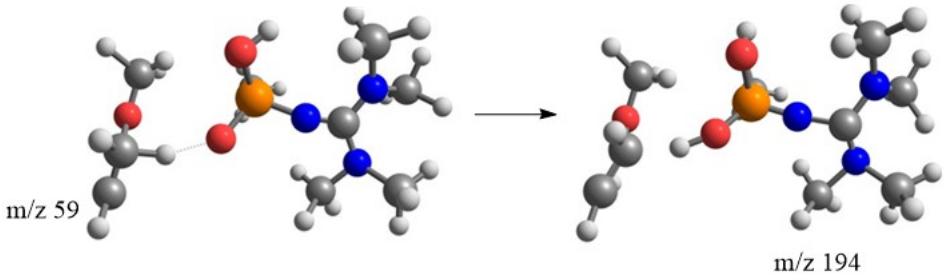

Figure 13 - Formation mechanism of the $C_6H_{17}N_3O_2P^+$ ion (*m/z* 194)

However, a *m/z* 193 fragment ion of considerable intensity can be observed in the theoretical spectra, in contrast with its absence in the experiment. The presence of this *m/z* 193 peak compared to the experiment results from the overestimation of the statistical charge assigned to the complimentary $C_6H_{16}N_3O_2P$ fragment, which is expected to be neutral during the cleavage of the O-methoxyethyl bond.

Most fragmentations of the studied compound originate from the fragment ion $C_7H_{16}N_2O_3P^+$ (*m/z* 207), formed by elimination from Protomer III, which are discussed in the next paragraphs. The $C_4H_{10}N_2OP^+$(*m/z* 133), $C_4H_{10}O_3P^+$ (*m/z* 137) and $C_4H_{10}N_2O_2P^+$ (*m/z* 149)

ions were found to originate from this ion. The *m/z* 149 ion is formed in a McLafferty-type rearrangement as shown in Figure 12 and no further fragmentation was observed from it.

After a nitrogen attack on phosphorus, the *m/z* 137 ion undergoes a 5-ring rearrangement (Figure 14), generating an intermediate that originates either the *m/z* 93 or the *m/z* 111 fragments. Production of the *m/z* 111 ion involves a McLafferty-type rearrangement that eliminates ethyne, while the *m/z* 93 ion is formed by a CMF that releases acetaldehyde. A different path from ion *m/z* 137, in which a proton is transferred from the terminal carbon to the phosphorus atom, generates an alternative structure for ion *m/z* 93 that releases formaldehyde to produce *m/z* 63 ion.

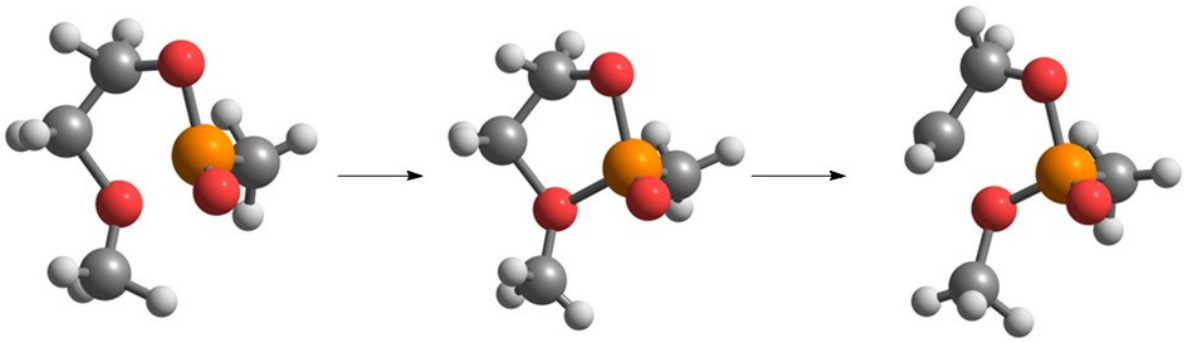

Figure 14 – Five-ring rearrangement mechanism of the $C_4H_{10}O_3P^+$ ion (*m/z* 137)

The MD simulations indicated the formation of the *m/z* 133 ion through two mechanisms (Figure 12), both consisting of a combination of hydrogen migrations and CMF reactions. For protomer III, after the formation of the *m/z* 207 ion, it undergoes a hydrogen migration and eliminates 2-methoxyacetaldehyde by cleaving the P-O bond. For protomer IV, subsequently to the formation of *m/z* 176 ion, it also undergoes a hydrogen migration followed by elimination of N-methylmethanimine. After the formation of the *m/z* 133 ion, only in the protomer IV simulation was possible to verify the generation of the *m/z* 71 ion in a CRF mechanism by eliminating the neutral methyl(oxo)phosphane group.

Although one could infer that the *m/z* 106 ion generated in the ESI-CID mode has a structure similar to the one proposed in the literature [13] for the fragment generated by EI, the results indicate the occurrence of a rearrangement in the *m/z* 176 ion, with the transfer of the dimethylamino group from carbon to phosphorus, as shown in Figure 15, followed by cleavage eliminating N,N-dimethylcyanamide.

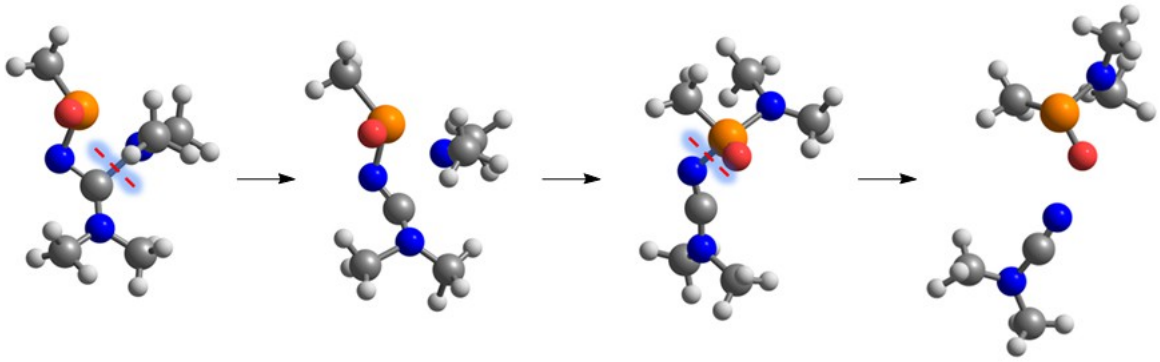

Figure 15 - Formation mechanism of $C_3H_9NOP^+$ ion (*m/z* 106)

As expected, shorter simulation than reaction times can lead to an underrepresentation of slower dissociation events [38]. This is indicated by underestimating the *m/z* 137 ion compared to the greater intensity of the *m/z* 207 ion from which it derives compared to the experiment. Moreover, this results in the observed small unmatched signals in the theoretical spectrum since it favors an overestimation in survival rates of non-physical artifacts [38].

Although not typically considered in fragmentation trees, selected molecules under ESI conditions can have their even-electron ions generated in the ESI source produce radical cations (odd-electron ions) by homolytic cleavage under CID conditions [22]. The homolytic cleavage of the P-N bond (Figure 16) eliminates a neutral 2-methyl-1,3,2-dioxaphospholane 2-oxide molecule, allowing the positive charge to stay with the 1,1,3,3-tetramethylguanidine radical ion of *m/z* 115.

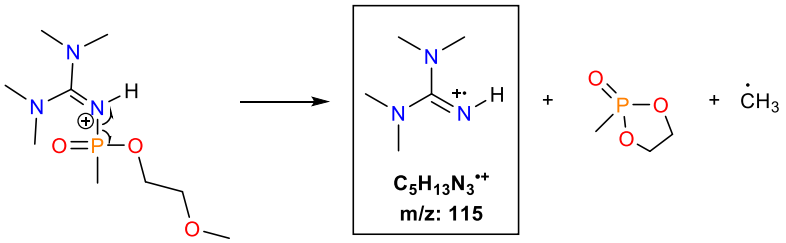

Figure 16 - Formation mechanism of $C_5H_{13}N_3^{\bullet+}$ (*m/z* 115) radical ion.

Nonetheless, most of the *m/z* 115 ion signals determined by the MD simulations were due to another mechanism, consisting of the cleavage of the original protonated ion (*m/z* 252) into the *m/z* 137 and *m/z* 115 fragments. For protomer II, this produces a charged *m/z* 115 fragment $C_5H_{13}N_3^{\bullet+}$, as the positive charge stays in the 1,1,3,3-tetramethylguanidine side of the ion. This overestimates the ion *m/z* 115 compared to the experiment and underestimates the intensity of the complimentary *m/z* 137 ion, which would be formed if the reaction occurred by a heterolytic cleavage in a classic ESI charge migration mechanism. However, this option was not observed for the protomer III, and the preferential fragmentation pathway is towards the generation of *m/z* 207 and, subsequently, ion *m/z* 137.

Although not identified by QCxMS, the formation of fragment 85 possibly involves a methyl migration between the neighboring atoms C-N-C-N of the *m/z* 115 ion, as depicted in Figure 17.

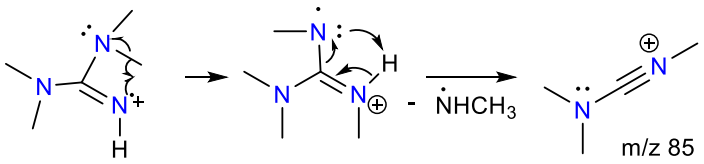

Figure 17 - Proposed fragmentation pathway from fragment 8 to fragment 4, which was not identified by QCxMS.

A radical elimination of a hydrogen radical from the studied molecule leads to the formation of the *m/z* 251 radical ion, which is observed in the experimental spectrum (Figure 18). The final part of the spectrum consists of the protonated ion (*m/z* 252) ion.

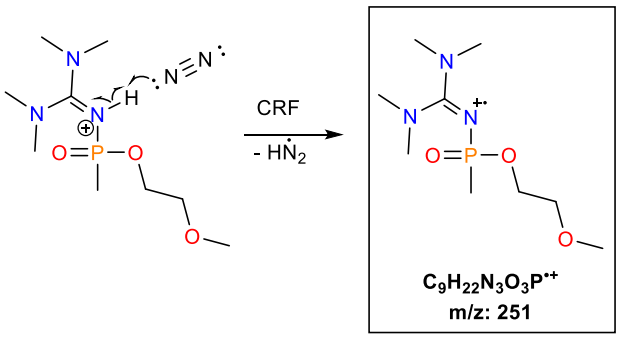

Figure 18 - Formation mechanism of $C_9H_{22}N_3O_3P^{\bullet+}$ (*m/z* 251)

Movies for all the fragmentation mechanisms discussed in the text are provided in the Supporting Information.

4 CONCLUSIONS

In the present study, O-2-methoxyethyl N-[bis(dimethylamino)methylidene]-P-methylphosphonamidate molecule was prepared through micro synthetic protocols, and its mass spectra were studied by EI-MS and ESI-MS/MS techniques. Moreover, the fragmentation pathways of the experimental ESI-MS/MS spectra were described using empirical rules with the help of the trajectories obtained through molecular dynamics simulations in CID positive ion mode. The protomers with the largest population within a defined energy window of 30 kcal/mol were used as starting points to calculate corresponding MS/MS spectra, achieving a coverage > 93% of the measured signals compared to the experimental spectrum.

ACKNOWLEDGMENTS

We thank Prof. Norberto Peporine Lopes (USP, Ribeirão Preto) for valuable discussions concerning the fragmentation mechanisms and Prof. Stefan Grimme (Bonn University) for kindly making available the QCxMS program. I. B. thanks the Brazilian agencies CNPq (Grant numbers 304148/2018-0 and 409447/2018-8) and FAPERJ (Grant number E26/201.197/2021) for support. We thank the Brazilian Army for supporting this research.

AUTHOR CONTRIBUTIONS

Taynara Carvalho-Silva: Formal analysis, Visualization, Investigation, Writing – Original Draft. **Lucas Modesto-Costa**: Software. **Caio V. N. Borges**: Resources. **Samir F. A. Cavalcante**: Methodology, Writing – Review & Editing. **Roberto B. Sousa:** Conceptualization, Supervision, Writing – Review & Editing. **Antonio L. S. Lima:** Conceptualization, Writing – Review & Editing. **Itamar Borges Jr.:** Conceptualization, Funding Acquisition, Methodology, Visualization, Resources, Writing – Review & Editing.

REFERENCES

[1] OPCW, Convention on the Prohibition of the Development, Production, Stockpiling and Use of Chemical Weapons and on their Destruction, (1993). https://doi.org/10.1515/9783110874815-026.

[2] S. Cavalcante, D. Kitagawa, R. Rodrigues, T. Silva, L. Bernardo, A.B. Correa, A. Simas, One-Pot Synthesis of NEMP, a VX Surrogate, and Reactivation of NEMP-Inhibited Electrophorus Eel Acetylcholinesterase by Current Antidotes, J. Braz. Chem. Soc. (2018). https://doi.org/10.21577/0103-5053.20180246.

[3] V. Aroniadou-Anderjaska, J.P. Apland, T.H. Figueiredo, M. De Araujo Furtado, M.F. Braga, Acetylcholinesterase inhibitors (nerve agents) as weapons of mass destruction: History, mechanisms of action, and medical countermeasures, Neuropharmacology. 181 (2020) 108298. https://doi.org/10.1016/j.neuropharm.2020.108298.

[4] M. Kloske, Z. Witkiewicz, Novichoks – The A group of organophosphorus chemical warfare agents, Chemosphere. 221 (2019) 672–682. https://doi.org/10.1016/j.chemosphere.2019.01.054.

[5] V.S. Mirzayanov, State secrets: an insider's chronicle of the Russian chemical weapons program, Outskirts Press, Inc, Denver, Colorado, 2009.
[6] T.C.C. França, D.A.S. Kitagawa, S.F. de A. Cavalcante, J.A.V. da Silva, E. Nepovimova, K. Kuca, Novichoks: The dangerous fourth generation of chemical weapons, International Journal of Molecular Sciences. 20 (2019). https://doi.org/10.3390/ijms20051222.
[7] M. Kloske, Z. Witkiewicz, Novichoks – The A group of organophosphorus chemical warfare agents, Chemosphere. 221 (2019) 672–682. https://doi.org/10.1016/j.chemosphere.2019.01.054.
[8] Science, Poisoning of Putin opponent renews spotlight on deadly Russian chemical weapon, (2020). https://www.science.org/content/article/poisoning-putin-opponent-renews-spotlight-deadly-russian-chemical-weapon (accessed October 16, 2021).
[9] R. Stone, U.K. attack puts nerve agent in the spotlight, Science. 359 (2018) 1314–1315. https://doi.org/10.1126/science.359.6382.1314.
[10] Costanzi Research, A Historical Event: Chemicals Added to CWC Schedule 1, Costanzi Research. (2019). https://costanziresearch.com/cw-nonproliferation/cw-control-lists/cwc-schedule-1-amendment/ (accessed October 17, 2021).
[11] S. Costanzi, G.D. Koblentz, Updating the CWC: How We Got Here and What Is Next | Arms Control Association, (2020). https://www.armscontrol.org/act/2020-04/features/updating-cwc-we-got-here-what-next (accessed October 16, 2021).
[12] OPCW, Consolidated Text of Adopted Changes to Schedule 1 of the Annex on Chemicals to the Chemical Weapons Convention, (2019). https://www.opcw.org/sites/default/files/documents/2019/12/s-1820-2019%28e%29.pdf (accessed October 16, 2021).
[13] S.E. Hosseini, H. Saeidian, A. Amozadeh, M.T. Naseri, M. Babri, Fragmentation pathways and structural characterization of organophosphorus compounds related to the Chemical Weapons Convention by electron ionization and electrospray ionization tandem mass spectrometry: Mass spectral studies of organophosphorus compounds related to CWC, Rapid Commun. Mass Spectrom. 30 (2016) 2585–2593. https://doi.org/10.1002/rcm.7757.
[14] Jonathan Oyler, Kathleen Maistros, Benjamin Oyler, David Kilgour, Liquid Chromatography–Mass Spectrometry in Analysis of Chemicals Related to the ChemicalWeapons Convention, in: Encyclopedia of Analytical Chemistry: Applications, Theory and Instrumentation, 1st ed., Wiley, 2006. https://doi.org/10.1002/9780470027318.
[15] R.M. Black, R.W. Read, Liquid Chromatography/Mass Spectrometry in Analysis of Chemicals Related to the Chemical Weapons Convention, in: Chemical Weapons Convention Chemicals Analysis, John Wiley & Sons, Ltd, 2005: pp. 283–320. https://doi.org/10.1002/0470012285.ch12.
[16] P. Vanninen, Recommended Operating Procedures for Analysis in the Verification of Chemical Disarmament, 2017.
[17] J.Y. Lee, K.C. Lim, H.S. Kim, Characterization and Study on Fragmentation Pathways of a Novel Nerve Agent, 'Novichok (A234)', in Aqueous Solution by Liquid Chromatography–Tandem Mass Spectrometry, Molecules. 26 (2021) 1059. https://doi.org/10.3390/molecules26041059.
[18] M. Otsuka, H. Miyaguchi, M. Uchiyama, Analysis of degradation products of nitrogen mustards via hydrophilic interaction liquid chromatography–tandem mass spectrometry, Journal of Chromatography A. 1602 (2019) 199–205. https://doi.org/10.1016/j.chroma.2019.05.015.
[19] H. Saeidian, S.E. Hosseini, A. Amoozadeh, M.T. Naseri, M. Babri, Investigation of sarin(Se) reactivity against human plasma proteins using liquid chromatography-tandem

mass spectrometry, J Mass Spectrom. 53 (2018) 138–145. https://doi.org/10.1002/jms.4045.
[20] S. Banerjee, S. Mazumdar, Electrospray Ionization Mass Spectrometry: A Technique to Access the Information beyond the Molecular Weight of the Analyte, International Journal of Analytical Chemistry. 2012 (2012) 1–40. https://doi.org/10.1155/2012/282574.
[21] J. Fenn, M. Mann, C. Meng, S. Wong, C. Whitehouse, Electrospray ionization for mass spectrometry of large biomolecules, Science. 246 (1989) 64–71. https://doi.org/10.1126/science.2675315.
[22] D.P. Demarque, A.E.M. Crotti, R. Vessecchi, J.L.C. Lopes, N.P. Lopes, Fragmentation reactions using electrospray ionization mass spectrometry: an important tool for the structural elucidation and characterization of synthetic and natural products, Nat. Prod. Rep. 33 (2016) 432–455. https://doi.org/10.1039/C5NP00073D.
[23] A. Steckel, G. Schlosser, An Organic Chemist's Guide to Electrospray Mass Spectrometric Structure Elucidation, Molecules. 24 (2019) 611. https://doi.org/10.3390/molecules24030611.
[24] P.A. D'Agostino, Chapter 25 Chemical warfare agents, in: Handbook of Analytical Separations, Elsevier, 2008: pp. 839–872. https://doi.org/10.1016/S1567-7192(06)06025-6.
[25] E.W.J. Hooijschuur, A.G. Hulst, A.L. de Jong, L.P. de Reuver, S.H. van Krimpen, E.R.J. Wils, C.E. Kientz, Identification of chemicals related to the chemical weapons convention during an interlaboratory proficiency test, Trends in Analytical Chemistry. 21 (2002) 15. https://doi.org/10.1016/S0165-9936(01)00140-6.
[26] F.C.S. Chernicharo, L. Modesto-Costa, I. Borges, Molecular dynamics simulation of the electron ionization mass spectrum of tabun, J Mass Spectrom. 55 (2020) e4513. https://doi.org/10.1002/jms.4513.
[27] G.R. Silva, I. Borges Jr., J.D. Figueroa-Villar, A.T. de Castro, Defesa química: histórico, classificação dos agentes de guerra e ação dos neurotóxicos, Quím. Nova. 35 (2012) 2083–2091. https://doi.org/10.1590/S0100-40422012001000033.
[28] L. Modesto-Costa, S.T. Martinez, A.C. Pinto, R. Vessecchi, I. Borges, Elucidating the mass spectrum of the retronecine alkaloid using DFT calculations, J Mass Spectrom. 53 (2018) 934–941. https://doi.org/10.1002/jms.4253.
[29] V. Ásgeirsson, C.A. Bauer, S. Grimme, Quantum chemical calculation of electron ionization mass spectra for general organic and inorganic molecules, Chem. Sci. 8 (2017) 4879–4895. https://doi.org/10.1039/C7SC00601B.
[30] P. de Sainte Claire, W.L. Hase, Thresholds for the Collision-Induced Dissociation of Clusters by Rare Gas Impact, J. Phys. Chem. 100 (1996) 8190–8196. https://doi.org/10.1021/jp953622t.
[31] K. Song, R. Spezia, Theoretical mass spectrometry: tracing ions with classical trajectories, De Gruyter, Berlin ; Boston, 2018.
[32] E. Martínez-Núñez, A. Fernández-Ramos, S.A. Vázquez, J.M.C. Marques, M. Xue, W.L. Hase, Quasiclassical dynamics simulation of the collision-induced dissociation of Cr(CO)6+ with Xe, The Journal of Chemical Physics. 123 (2005) 154311. https://doi.org/10.1063/1.2044687.
[33] Y. Djoumbou-Feunang, A. Pon, N. Karu, J. Zheng, C. Li, D. Arndt, M. Gautam, F. Allen, D.S. Wishart, CFM-ID 3.0: Significantly Improved ESI-MS/MS Prediction and Compound Identification, Metabolites. 9 (2019) 72. https://doi.org/10.3390/metabo9040072.
[34] J. Cautereels, M. Claeys, D. Geldof, F. Blockhuys, Quantum chemical mass spectrometry: ab initio prediction of electron ionization mass spectra and identification of new

fragmentation pathways, Journal of Mass Spectrometry. 51 (2016) 602–614. https://doi.org/10.1002/jms.3791.
[35] J. Koopman, S. Grimme, Calculation of Electron Ionization Mass Spectra with Semiempirical GFNn-xTB Methods, ACS Omega. 4 (2019). https://doi.org/10.1021/acsomega.9b02011.
[36] F.C.S. Chernicharo, L. Modesto-Costa, I. Borges, Simulation of the electron ionization mass spectra of the Novichok nerve agent, J Mass Spectrom. 56 (2021). https://doi.org/10.1002/jms.4779.
[37] J. Koopman, S. Grimme, From QCEIMS to QCxMS: A Tool to Routinely Calculate CID Mass Spectra Using Molecular Dynamics, J. Am. Soc. Mass Spectrom. 32 (2021) 1735–1751. https://doi.org/10.1021/jasms.1c00098.
[38] R. Schnegotzki, J. Koopman, S. Grimme, R.D. Süssmuth, Quantum Chemistry-based Molecular Dynamics Simulations as a Tool for the Assignment of ESI-MS/MS Spectra of Drug Molecules, Chemistry A European J. 28 (2022). https://doi.org/10.1002/chem.202200318.
[39] J. Koopman, S. Grimme, Calculation of mass spectra with the QCxMS method for negatively and multiply charged molecules, Chemistry, 2022. https://doi.org/10.26434/chemrxiv-2022-w5260.
[40] P. Wright, A. Alex, T. Nyaruwata, T. Parsons, F. Pullen, Using density functional theory to rationalise the mass spectral fragmentation of maraviroc and its metabolites: Mass spectral fragmentation of maraviroc and its metabolites, Rapid Commun. Mass Spectrom. 24 (2010) 1025–1031. https://doi.org/10.1002/rcm.4458.
[41] A. Galezowska, M.W. Harrison, J.M. Herniman, C.-K. Skylaris, G.J. Langley, A predictive science approach to aid understanding of electrospray ionisation tandem mass spectrometric fragmentation pathways of small molecules using density functional calculations: Understanding ESI-MS/MS fragmentation pathways using FDC, Rapid Commun. Mass Spectrom. 27 (2013) 964–970. https://doi.org/10.1002/rcm.6536.
[42] S. Pratihar, M.C. Nicola Barbosa Muniz, X. Ma, I. Borges, W.L. Hase, Pronounced changes in atomistic mechanisms for the $Cl^- + CH_3 I S_N 2$ reaction with increasing collision energy, Phys. Chem. Chem. Phys. 21 (2019) 2039–2045. https://doi.org/10.1039/C8CP06198J.
[43] Z. Homayoon, V. Macaluso, A. Martin-Somer, M.C.N.B. Muniz, I. Borges, W.L. Hase, R. Spezia, Chemical dynamics simulations of CID of peptide ions: comparisons between $TIK(H^+)_2$ and $TLK(H^+)_2$ fragmentation dynamics, and with thermal simulations, Phys. Chem. Chem. Phys. 20 (2018) 3614–3629. https://doi.org/10.1039/C7CP06818B.
[44] H. Bhakhoa, L. Rhyman, P. Ramasami, Theoretical study of the molecular aspect of the suspected novichok agent A234 of the Skripal poisoning, R. Soc. Open Sci. 6 (2019) 181831. https://doi.org/10.1098/rsos.181831.
[45] Y.A. Imrit, H. Bhakhoa, T. Sergeieva, S. Danés, N. Savoo, M.I. Elzagheid, L. Rhyman, D.M. Andrada, P. Ramasami, A theoretical study of the hydrolysis mechanism of A-234; the suspected novichok agent in the Skripal attack, RSC Adv. 10 (2020) 27884–27893. https://doi.org/10.1039/D0RA05086E.
[46] L.A. Vieira, J.S.F.D. Almeida, T.C.C. França, I. Borges, Electronic and spectroscopic properties of A-series nerve agents, Computational and Theoretical Chemistry. 1202 (2021) 113321. https://doi.org/10.1016/j.comptc.2021.113321.
[47] Y. Tan, I. Tay, L. Loy, K. Aw, Z. Ong, S. Manzhos, A Scheme for Ultrasensitive Detection of Molecules with Vibrational Spectroscopy in Combination with Signal Processing, Molecules. 24 (2019) 776. https://doi.org/10.3390/molecules24040776.
[48] K. Jeong, J. Choi, Theoretical study on the toxicity of 'Novichok' agent candidates, R. Soc. Open Sci. 6 (2019) 190414. https://doi.org/10.1098/rsos.190414.

[49] I. Lyagin, E. Efremenko, Theoretical evaluation of suspected enzymatic hydrolysis of Novichok agents, Catalysis Communications. 120 (2019) 91–94. https://doi.org/10.1016/j.catcom.2018.11.019.
[50] P. Pracht, F. Bohle, S. Grimme, Automated exploration of the low-energy chemical space with fast quantum chemical methods, Phys. Chem. Chem. Phys. 22 (2020) 7169–7192. https://doi.org/10.1039/C9CP06869D.
[51] P. Pracht, C.A. Bauer, S. Grimme, Automated and efficient quantum chemical determination and energetic ranking of molecular protonation sites, Journal of Computational Chemistry. 38 (2017) 2618–2631. https://doi.org/10.1002/jcc.24922.
[52] S. Grimme, Exploration of Chemical Compound, Conformer, and Reaction Space with Meta-Dynamics Simulations Based on Tight-Binding Quantum Chemical Calculations, J. Chem. Theory Comput. 15 (2019) 2847–2862. https://doi.org/10.1021/acs.jctc.9b00143.
[53] C. Bannwarth, S. Ehlert, S. Grimme, GFN2-xTB—An Accurate and Broadly Parametrized Self-Consistent Tight-Binding Quantum Chemical Method with Multipole Electrostatics and Density-Dependent Dispersion Contributions, J. Chem. Theory Comput. 15 (2019) 1652–1671. https://doi.org/10.1021/acs.jctc.8b01176.
[54] S. Grimme, J.G. Brandenburg, C. Bannwarth, A. Hansen, Consistent structures and interactions by density functional theory with small atomic orbital basis sets, J Chem Phys. 143 (2015) 054107. https://doi.org/10.1063/1.4927476.
[55] F. Weigend, Accurate Coulomb-fitting basis sets for H to Rn, Phys. Chem. Chem. Phys. 8 (2006) 1057. https://doi.org/10.1039/b515623h.
[56] S. Grimme, F. Bohle, A. Hansen, P. Pracht, S. Spicher, M. Stahn, Efficient Quantum Chemical Calculation of Structure Ensembles and Free Energies for Nonrigid Molecules, J. Phys. Chem. A. 125 (2021) 4039–4054. https://doi.org/10.1021/acs.jpca.1c00971.
[57] F. Neese, The ORCA program system, WIREs Computational Molecular Science. 2 (2012) 73–78. https://doi.org/10.1002/wcms.81.
[58] F. Neese, Software update: The ORCA program system—Version 5.0, WIREs Comput Mol Sci. 12 (2022). https://doi.org/10.1002/wcms.1606.
[59] F. Neese, F. Wennmohs, U. Becker, C. Riplinger, The ORCA quantum chemistry program package, J. Chem. Phys. 152 (2020) 224108. https://doi.org/10.1063/5.0004608.
[60] C. Bannwarth, E. Caldeweyher, S. Ehlert, A. Hansen, P. Pracht, J. Seibert, S. Spicher, S. Grimme, Extended tight-binding quantum chemistry methods, WIREs Comput Mol Sci. 11 (2021). https://doi.org/10.1002/wcms.1493.
[61] R.O. Jones, O. Gunnarsson, The density functional formalism, its applications and prospects, Rev. Mod. Phys. 61 (1989) 689–746. https://doi.org/10.1103/RevModPhys.61.689.
[62] Visualization — xtb doc 2023 documentation, (n.d.). https://xtb-docs.readthedocs.io/en/latest/qcxms_doc/qcxms_plot.html (accessed February 6, 2023).
[63] M. Verstraete, X. Gonze, Smearing scheme for finite-temperature electronic-structure calculations, Phys. Rev. B. 65 (2001) 035111. https://doi.org/10.1103/PhysRevB.65.035111.
[64] Running QCxMS — xtb doc 2021 documentation, (n.d.). https://xtb-docs.readthedocs.io/en/latest/qcxms_doc/qcxms_run.html (accessed October 19, 2021).
[65] A. Schwarzenberg, F. Ichou, R.B. Cole, X. Machuron-Mandard, C. Junot, D. Lesage, J.-C. Tabet, Identification tree based on fragmentation rules for structure elucidation of organophosphorus esters by electrospray mass spectrometry: Structure elucidation of organophosphorus esters, J. Mass Spectrom. 48 (2013) 576–586. https://doi.org/10.1002/jms.3180.